

Infection Susceptibility in Gastric Intrinsic Factor (Vitamin B₁₂)-Defective Mice Is Subject to Maternal Influences

Lynda Mottram,^a Anneliese O. Speak,^a Reza M. Selek,^{b,c} Emma L. Cambridge,^a Zoe McIntyre,^a Leanne Kane,^a Subhankar Mukhopadhyay,^a Carolyn Grove,^a Amy Colin,^a Cordelia Brandt,^a Maria A. Duque-Correa,^a Jessica Forbester,^a Tu Anh Pham Nguyen,^a Christine Hale,^a George S. Vasiliou,^a Mark J. Arends,^d Brendan W. Wren,^e Gordon Dougan,^a Simon Clare^a

Wellcome Trust Sanger Institute, Wellcome Trust Genome Campus, Hinxton, United Kingdom^a; Wellcome Trust Genome Campus, European Bioinformatics Institute, Cheminformatics and Metabolism, Hinxton, United Kingdom^b; Department of Biochemistry and Cambridge Systems Biology Centre, University of Cambridge, Cambridge, United Kingdom^c; Division of Pathology, University Of Edinburgh, Edinburgh, United Kingdom^d; Department of Pathogen Molecular Biology, London School of Hygiene and Tropical Medicine, London, United Kingdom^e

G.D. and S.C. contributed equally to this report.

ABSTRACT Mice harboring a mutation in the gene encoding gastric intrinsic factor (Gif), a protein essential for the absorption of vitamin B₁₂/cobalamin (Cbl), have potential as a model to explore the role of vitamins in infection. The levels of Cbl in the blood of *Gif*^{tm1a/tm1a} mutant mice were influenced by the maternal genotype, with offspring born to heterozygous (high Cbl, F₁) mothers exhibiting a significantly higher serum Cbl level than those born to homozygous (low Cbl, F₂) equivalents. Low Cbl levels correlated with susceptibility to an infectious challenge with *Salmonella enterica* serovar Typhimurium or *Citrobacter rodentium*, and this susceptibility phenotype was moderated by Cbl administration. Transcriptional and metabolic profiling revealed that Cbl deficient mice exhibited a bioenergetic shift similar to a metabolic phenomenon commonly found in cancerous cells under hypoxic conditions known as the Warburg effect, with this metabolic effect being exacerbated further by infection. Our findings demonstrate a role for Cbl in bacterial infection, with potential general relevance to dietary deficiency and infection susceptibility.

IMPORTANCE Malnutrition continues to be a major public health problem in countries with weak infrastructures. In communities with a high prevalence of poor diet, malnourishment and infectious disease can impact vulnerable individuals such as pregnant women and children. Here, we describe a highly flexible murine model for monitoring maternal and environmental influences of vitamin B₁₂ metabolism. We also demonstrate the potential importance of vitamin B₁₂ in controlling susceptibility to bacterial pathogens such as *C. rodentium* and *S. Typhimurium*. We postulate that this model, along with similarly vitamin deficient mice, could be used to further explore the mechanisms associated with micronutrients and susceptibility to diseases, thereby increasing our understanding of disease in the malnourished.

Received 12 May 2016 Accepted 13 May 2016 Published 21 June 2016

Citation Mottram L, Speak AO, Selek RM, Cambridge EL, McIntyre Z, Kane L, Mukhopadhyay S, Grove C, Colin A, Brandt C, Duque-Correa MA, Forbester J, Nguyen TAP, Hale C, Vasiliou GS, Arends MJ, Wren BW, Dougan G, Clare S. 2016. Infection susceptibility in gastric intrinsic factor (vitamin B₁₂)-defective mice is subject to maternal influences. *mBio* 7(3):e00830-16. doi:10.1128/mBio.00830-16.

Editor Philippe J. Sansonetti, Pasteur Institute

Copyright © 2016 Mottram et al. This is an open-access article distributed under the terms of the [Creative Commons Attribution 4.0 International license](https://creativecommons.org/licenses/by/4.0/).

Address correspondence to Simon Clare, SC7@sanger.ac.uk.

This article is a direct contribution from a Fellow of the American Academy of Microbiology. External solicited reviewers: William Jacobs, Albert Einstein College of Medicine; Brett Finlay, University of British Columbia.

Clinical and epidemiological studies have demonstrated an association of malnutrition, dietary deficiency, and infection (1, 2). Infections are more frequent and can be more chronic in primary malnourished individuals (2, 3), with evidence suggesting that infection further weakens the host by reducing nutrient uptake and impeding the ability to mount an effective immune response (4–6). However, relatively little is known about the physiological and immunological signatures linking general malnutrition or specific dietary deficiencies to infection susceptibility.

Vitamin B₁₂ (cobalamin [Cbl]) serves as an essential cofactor in the cellular growth of most prokaryotic organisms. While bacterial species such as *Escherichia coli* and *Salmonella enterica* have the ability to produce Cbl *de novo* anaerobically, mammals obtain Cbl exclusively from animal protein dietary sources (7). Mamma-

lian Cbl absorption is a highly specific process, with the secreted protein gastric intrinsic factor (Gif) being responsible for transporting Cbl through the small intestine and facilitating endocytosis in the distal ileum (8). In humans, Cbl deficiency is linked to a variety of clinical conditions, including megaloblastic anemia, optic atrophy, degeneration of the spinal cord, renal abnormalities, and malabsorption (8–11). The impact of Cbl deficiency is likely multifactorial, as it normally plays a role in cellular metabolism with DNA stress, cellular oxidative damage, alterations in odd-chain fatty acid and cholesterol synthesis, and anaplerosis as consequences (8, 12–15).

We have recently shown that mice lacking Gif exhibit significant growth retardation and low bone mass, with the penetrance of this phenotype showing maternal influences (16). Here we

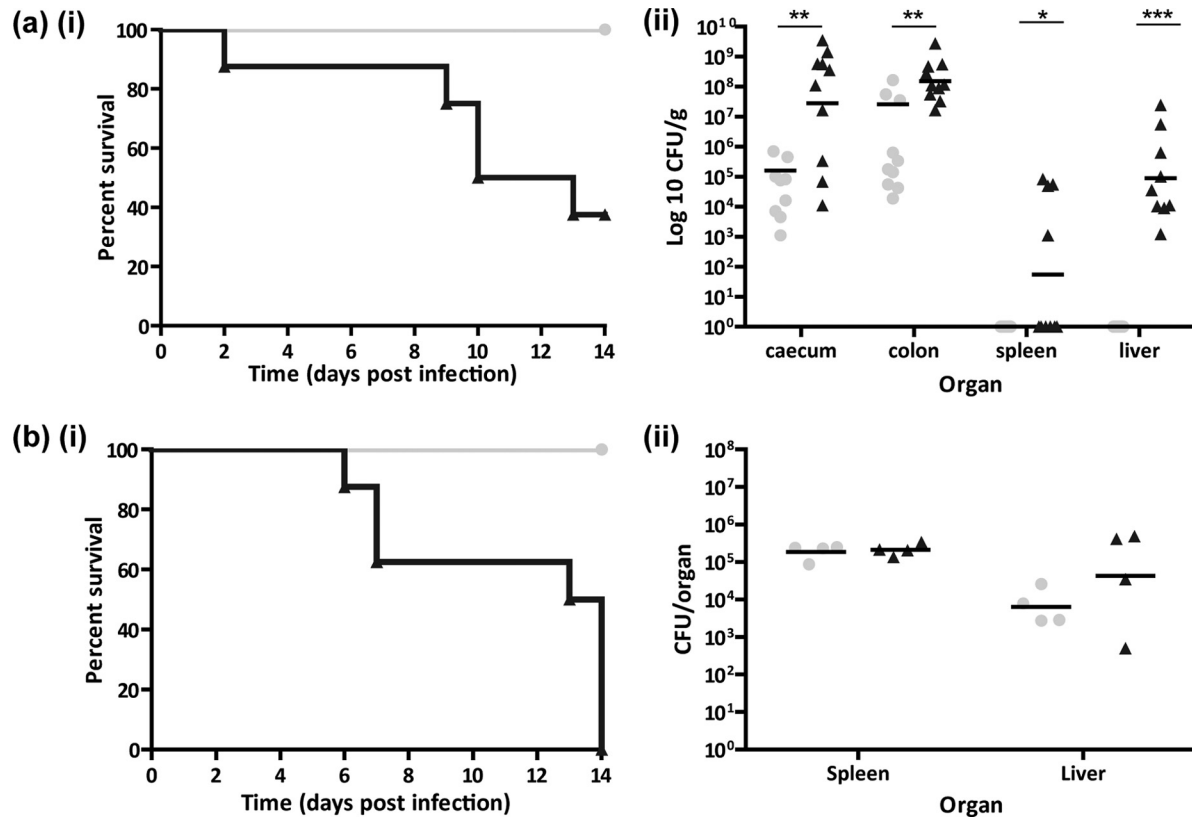


FIG 2 F_2 $Gif^{tm1a/tm1a}$ mice are susceptible to *C. rodentium* and *S. Typhimurium* pathogen challenges. (a, part i) Kaplan-Meier curve showing percent survival following infection of F_2 $Gif^{tm1a/tm1a}$ and wild-type mice with *C. rodentium* ($n = 8$). (a, part ii) Enumeration of *C. rodentium* bacteria in cecal, colon, spleen, and liver tissues of surviving F_2 $Gif^{tm1a/tm1a}$ and wild-type mice at day 14 p.i. (b, part i) Kaplan-Meier curve showing percent survival following infection of F_2 $Gif^{tm1a/tm1a}$ and wild-type mice with *S. Typhimurium* ($n = 8$). (b, part ii) Enumeration of *S. Typhimurium* bacteria in the spleens and livers of F_2 $Gif^{tm1a/tm1a}$ and wild-type mice at day 14 p.i. Gray circles represent wild-type mice. Black triangles represent F_2 $Gif^{tm1a/tm1a}$ mice. Black bars represent geometric mean values. ***, $P < 0.001$; **, $P < 0.01$; *, $P < 0.05$ (ANOVA with Dunn's multiple-comparison *post hoc* test).

F_2 $Gif^{tm1a/tm1a}$ mice are deficient in Cbl and have alterations in red blood cell and plasma chemistry. To ascertain if $Gif^{tm1a/tm1a}$ mice were Cbl deficient, we measured the blood plasma Cbl concentrations of wild-type and $Gif^{tm1a/tm1a}$ mice (Fig. 1d). We found that all of the wild-type mice exhibited high plasma Cbl concentrations ($\geq 2,000$ ng/liter), with F_1 $Gif^{tm1a/tm1a}$ mice showing various levels of blood plasma Cbl deficiency. However, blood plasma from F_2 $Gif^{tm1a/tm1a}$ mice consistently exhibited at least 20-fold lower Cbl levels than that from their wild-type counterparts (Fig. 1d). Further blood analysis showed that naive F_2 $Gif^{tm1a/tm1a}$ mice exhibited phenotypes similar to those of humans with severe Cbl deficiency (9, 11), with these F_2 mice having consistently lower erythrocyte counts (see Fig. S1b, part i, in the supplemental material) and a greater mean corpuscular volume (MCV; see Fig. S1b, part ii) than equivalent F_1 $Gif^{tm1a/tm1a}$ and wild-type mice. Moreover, megakaryocytes found in the spleens of F_2 $Gif^{tm1a/tm1a}$ mice were often hyperlobulated with hypersegmented nuclei indicative of cell cycle irregularities compared to wild-type cells (see Fig. S1a) (11).

Furthermore, in comparison to blood plasma collected from equivalent F_1 $Gif^{tm1a/tm1a}$ and wild-type mice, blood plasma from F_2 $Gif^{tm1a/tm1a}$ mice exhibited alterations in multiple clinical chemistry parameters (Fig. S1c). We observed that the concentrations of iron, high-density lipoproteins, cholesterol, as well as albumin, glucose, and glycerol, were significantly lower in the blood

plasma of F_2 $Gif^{tm1a/tm1a}$ mice (Fig. S1c, parts i to vi). Interestingly the level of urea, a clinical marker of muscle damage, was found to be significantly higher in the blood plasma of F_2 $Gif^{tm1a/tm1a}$ mice than in that of F_1 $Gif^{tm1a/tm1a}$ and wild-type mice (see Fig. S2c, part vii, in the supplemental material).

F_2 $Gif^{tm1a/tm1a}$ mice are hypersusceptible to *C. rodentium* and *S. Typhimurium* challenges. When groups of F_2 $Gif^{tm1a/tm1a}$ and wild-type mice were challenged with *C. rodentium*, 60% of the F_2 $Gif^{tm1a/tm1a}$ mice succumbed to infection by day 14 postinfection (p.i.), compared to none of the wild-type mice (Fig. 2a, part i). Although the enumeration of *C. rodentium* was statistically significantly higher in all of the organs of the challenged F_2 $Gif^{tm1a/tm1a}$ mice than in the challenged wild-type mice at day 14 p.i. (Fig. 2a, part ii), the two groups had similar colon weights and general patterns of colonic hyperplasia (see Fig. S2 in the supplemental material). Significantly, however, *C. rodentium* was consistently found ($P < 0.001$) in the livers of F_2 $Gif^{tm1a/tm1a}$ mice (Fig. 2a, part ii). Furthermore, other bacterial taxa, such as *Staphylococcus* and *Escherichia*, were also present in their livers, suggesting that polymicrobial sepsis was occurring after a *C. rodentium* challenge in these F_2 $Gif^{tm1a/tm1a}$ mice (data not shown). Importantly, bacteria were not generally detected in the livers of wild-type mice before or after a *C. rodentium* challenge.

Similar groups of wild-type and F_2 $Gif^{tm1a/tm1a}$ mice were also challenged with moderately attenuated *S. Typhimurium* M525. F_2

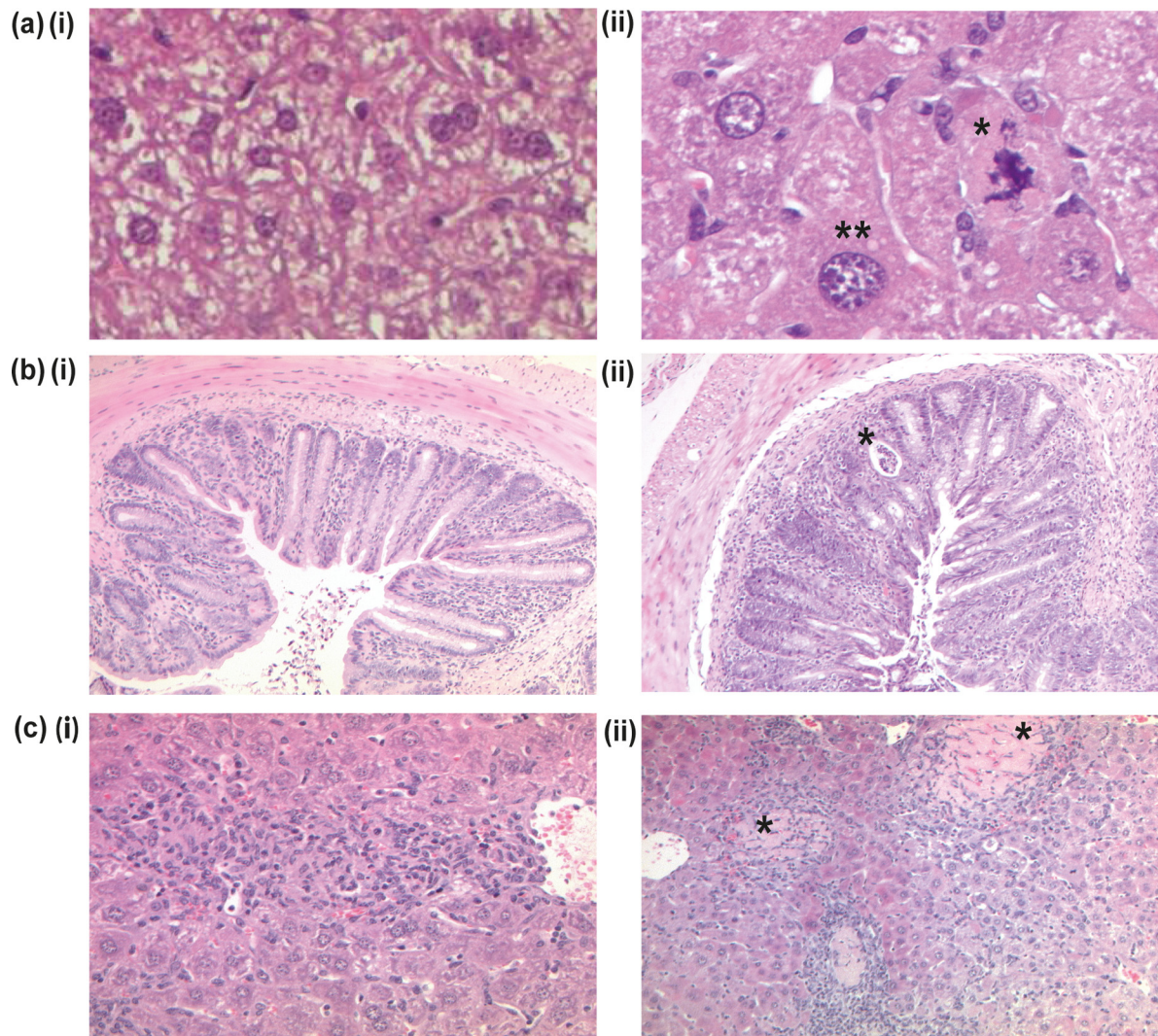


FIG 3 Representative hematoxylin- and eosin-stained sections from naive and infected F_2 $Gif^{tm1a/tm1a}$ and wild-type mice. (a) Liver sections from naive wild-type (i) and F_2 $Gif^{tm1a/tm1a}$ (ii) mice. A single asterisk indicates an abnormal mitotic figure, and double asterisks indicate enlarged cellular nuclei in an F_2 $Gif^{tm1a/tm1a}$ mouse ($\times 400$ magnification). (b) Colon sections obtained on day 14 after a *C. rodentium* challenge of wild-type (i) and F_2 $Gif^{tm1a/tm1a}$ (ii) mice. The asterisk indicates a crypt abscess in an F_2 $Gif^{tm1a/tm1a}$ mouse ($\times 100$ magnification). (c) Liver sections obtained on day 8 after an *S. Typhimurium* challenge of wild-type (i) and F_2 $Gif^{tm1a/tm1a}$ (ii) mice. Both images show inflammatory cellular infiltration and granuloma formation. Asterisks indicate the large necrotic regions seen in F_2 $Gif^{tm1a/tm1a}$ mice ($\times 200$ magnification).

$Gif^{tm1a/tm1a}$ mice showed signs of salmonellosis by day 4 p.i., with all mice having to be sacrificed between days 6 and 14 p.i. (Fig. 2b, part i). In contrast, wild-type mice exhibited little sign of disease and survived the challenge. Interestingly, the *S. Typhimurium* burdens in the spleens and livers of F_2 $Gif^{tm1a/tm1a}$ and wild-type mice were comparable at day 14 p.i. (Fig. 2b, part ii). Thus, overwhelming *S. Typhimurium* burdens were unlikely to be responsible for the disease in F_2 $Gif^{tm1a/tm1a}$ mice.

Histopathological signatures are observed in F_2 $Gif^{tm1a/tm1a}$ mice before and after a pathogen challenge. A detailed histopathological analysis of tissues from naive and pathogen-challenged F_2 $Gif^{tm1a/tm1a}$ and wild-type mice was performed. The general colonic and splenic morphology of naive F_2 $Gif^{tm1a/tm1a}$ mice was predominantly indistinguishable from that of wild-type mice (see Fig. S3a and b in the supplemental material). In contrast, F_2 $Gif^{tm1a/tm1a}$ mouse livers had hepatocytes with enlarged nuclei

and abnormal mitotic figures (Fig. 3a, part ii), indicating liver cell karyomegaly and mitotic impairment (18).

Although moderate inflammation and colonic pathology were present in wild-type mice at day 14 after a *C. rodentium* challenge (Fig. 3b, part i), F_2 $Gif^{tm1a/tm1a}$ mice developed a more severe epithelial inflammatory cell infiltration, accompanied by crypt abscesses containing neutrophils and intraepithelial lymphocytes in the mucosa and increased inflammation in the submucosa (Fig. 3b, part ii, for a higher magnification, and Fig. S3c, part i, in the supplemental material). Moreover, while the livers of wild-type mice challenged with *C. rodentium* showed no obviously enhanced inflammatory cell infiltrate, challenged F_2 $Gif^{tm1a/tm1a}$ mice exhibited rich inflammatory clusters particularly around the hepatic portal triad, with a thrombus occasionally present within the hepatic portal vein (see Fig. S3c, part ii).

The liver histology of F_2 $Gif^{tm1a/tm1a}$ mice challenged with

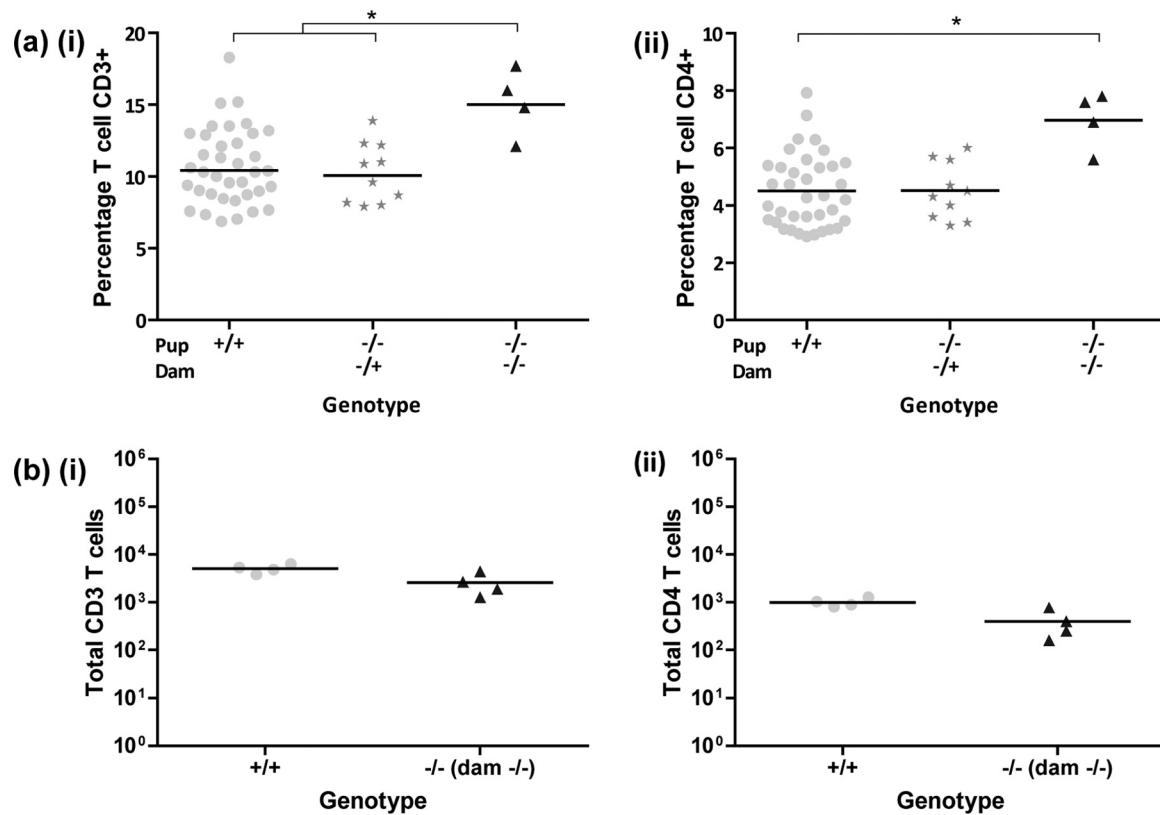


FIG 4 Immune cell profiling of naive and *S. Typhimurium*-challenged F₂ *Gif^{tm1a/tm1a}* and wild-type mice. (a) Analysis of peripheral blood leukocytes from 16-week-old naive mice showing percentages of CD3⁺ (i) and CD4⁺ (ii) T cells. (b) Analysis of spleen cells from *S. Typhimurium*-infected mice on day 14 p.i. for total CD3⁺ (i) and total CD4⁺ (ii) T cells. Samples were analyzed on a BD LSR Fortessa or BD LSR II apparatus. Interpretation of the results was performed with FlowJo v9. Black bars represent geometric mean values. *, $P < 0.05$ (one-way ANOVA followed by Dunn's multiple-comparison *post hoc* test).

S. Typhimurium exhibited evidence of significantly more damage than that of wild-type mice (Fig. 3c). Both groups of infected mice harbored clusters of macrophages forming granulomas; however, there were sizable areas of necrosis and regions of foamy fatty acid hepatocytes (fat vacuoles indicating metabolic stress) in the *S. Typhimurium* challenged F₂ *Gif^{tm1a/tm1a}* mice (Fig. 3c, part ii). The spleens of wild-type *S. Typhimurium* infected mice displayed a normal distribution of red and white pulp, but similarly challenged F₂ *Gif^{tm1a/tm1a}* mice exhibited increased extramedullary hematopoiesis with scattered large areas of necrosis with foci of macrophages in the red pulp compacting the white pulp (see Fig. S3d in the supplemental material).

Immune profiling of naive and *S. Typhimurium* infected F₂ *Gif^{tm1a/tm1a}* mice. We performed immune profiling before and after a challenge to identify immunological signatures associated with F₂ *Gif^{tm1a/tm1a}* mouse susceptibility to *S. Typhimurium* (19). While we found that the percentages of peripheral blood phagocytes and natural killer cells were broadly comparable (<http://www.mousephenotype.org/data/genes/MGI:1202394>), we did observe slight differences in the percentages of peripheral blood CD4⁺ and CD8⁺ T cells and CD4⁺ CD25⁺ regulatory T cells (Fig. 4a, part ii, and Fig. S4a in the supplemental material) in F₂ *Gif^{tm1a/tm1a}* mice and equivalent populations found in wild-type mice. However, when spleen leukocyte populations were analyzed at day 9 after *S. Typhimurium* infection, F₂ *Gif^{tm1a/tm1a}* mouse T cell populations (Fig. 4b), as well as all of the other lymphocyte

populations analyzed (see Fig. S4b), were comparable to those of similarly infected wild-type mice. Similarly, blood serum cytokine and chemokine analysis revealed no obvious differences between the concentrations of 25 different cytokines found in naive or infected F₂ *Gif^{tm1a/tm1a}* mice and those in wild-type mice (see Text S1 in the supplemental material for further details).

As macrophages are critical for the control of *Salmonella* replication and the homeostasis of granulomas *in vivo* (20, 21), we isolated macrophages from the peritoneal cavities of naive F₂ *Gif^{tm1a/tm1a}* and wild-type mice to evaluate their susceptibility to *S. Typhimurium*. We found that the ability of F₂ *Gif^{tm1a/tm1a}* macrophages to kill *S. Typhimurium* was not impaired and was comparable to that of wild-type macrophages. Interestingly, we found that F₂ *Gif^{tm1a/tm1a}* macrophages expressed higher levels of arginase 1 (see Fig. S4c in the supplemental material), a marker of alternatively activated M2 macrophages (6, 22).

Transcriptional profiling indicates potential cellular, metabolic, and anaplerosis pathway abnormalities in F₂ *Gif^{tm1a/tm1a}* mice. To identify changes in gene expression that could have an impact on the phenotype of F₂ *Gif^{tm1a/tm1a}* mice, microarray analysis was performed with mRNA prepared from the livers and colons of F₂ *Gif^{tm1a/tm1a}* and wild-type mice with or without a pathogen challenge. Genes differentially expressed ($P < 0.05$ with a 0.8-log-fold difference between F₂ *Gif^{tm1a/tm1a}* and wild-type mice) under each condition were further analyzed by Ingenuity Pathway Analysis (IPA; Qiagen, Redwood City, CA), enabling the

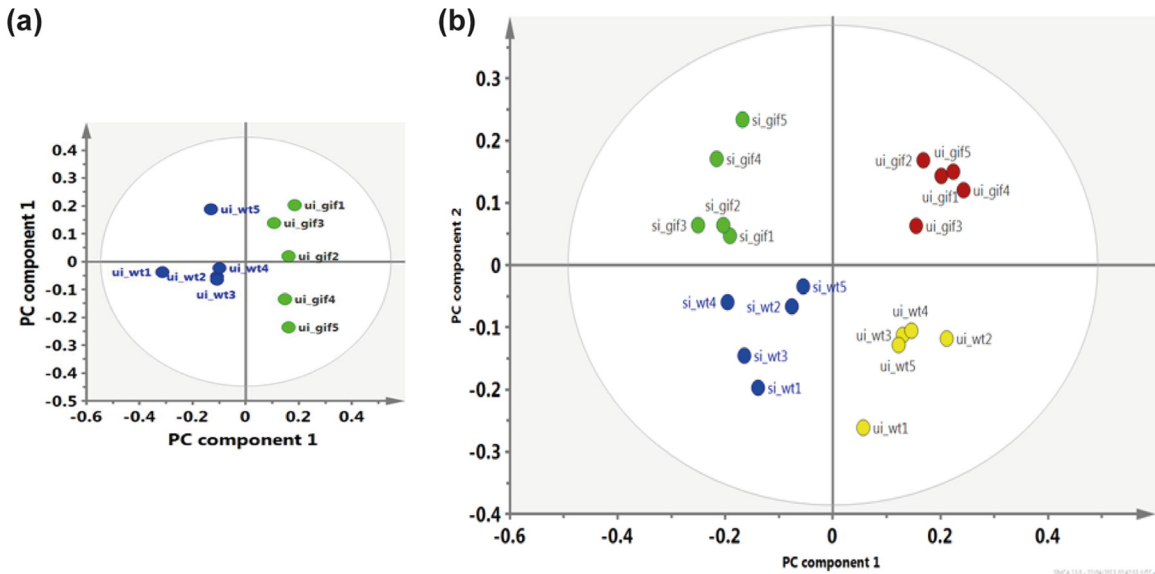


FIG 5 Metabotyping of blood serum from F₂ *Gif^{tm1a/tm1a}* and wild-type mice reveals metabolic abnormalities. (a) PCA score plot separating naive F₂ *Gif^{tm1a/tm1a}* mice (green circles) from naive wild-type mice (blue circles) with 92% of the variables explained (R^2_{cum}) by using the first four components with 72% predictability minus Q2. (b) Multivariate data analysis results comparing the blood serum of uninfected F₂ *Gif^{tm1a/tm1a}* (ui_gif; red circles) and wild-type (ui_wt; yellow circles) mice and that of *S. Typhimurium*-infected F₂ *Gif^{tm1a/tm1a}* (si_gif; green circles) and wild-type (si_wt; blue circles) mice. Principal component 1 discriminates on the basis of the presence or absence of infection, while principal component 2 separates different mouse genotypes, regardless of infection status. Ninety percent of the variables (R^2_{cum}) were explained by using the first five components with 73% predictability.

clustering of dysregulated mRNAs to specific biological and canonical pathways. Further, IPA upstream regulator analysis was used to predict potential upstream transcriptional regulators likely controlling these biological function and canonical pathways in the transcriptional data of the F₂ *Gif^{tm1a/tm1a}* mice.

Generally, differentially expressed genes in the colons of naive F₂ *Gif^{tm1a/tm1a}* mice were related to lipid metabolism, cell-to-cell signaling, molecular transport, small molecule biochemistry, and cell death and survival processes (see Dataset S1b in the supplemental material). Upstream regulator analysis predicted that genes associated with glycolysis regulation (*Por*, *Clock*, *Cry1*, and *Cry2*) (23, 24) (see Dataset S1a) might be controlling the functional gene profile in the colons of naive F₂ *Gif^{tm1a/tm1a}* mice. Functional gene categories in the livers of naive F₂ *Gif^{tm1a/tm1a}* mice were largely associated with lipid, vitamin, mineral, and nucleic acid metabolism, as well as cellular molecular transport (see Dataset S1c), with upstream regulator analysis predicting glycolysis and fatty acid synthesis associated genes (*Gpd1*, *Slc25a13*, *RorC*, *RorA*, and *Acox1*; see Dataset S1a) as potential regulators of disrupted cellular and biological functions in the livers of naive F₂ *Gif^{tm1a/tm1a}* mice. In particular, *Acox1* (encodes acyl coenzyme A [acyl-CoA] oxidase 1, palmitoyl), a peroxisome beta-oxidation fatty acid pathway regulator (25, 26), was predicted by IPA to be the most statically activated of the upstream transcriptional regulators (see Dataset S1a).

Of the differentially expressed genes identified in colonic mRNA of F₂ *Gif^{tm1a/tm1a}* mice challenged with *C. rodentium*, 60 were functionally associated with cell death and survival, with IPA predicting functional pathways associated with organismal injury and renal failure to be the most activated of these categories (see Dataset S1d in the supplemental material). Upstream transcriptional regulator analysis highlighted *Ptger4*, a prostaglandin regulator of mucosal integrity and suppressor of innate immunity

(27), as comparatively activated (see Dataset S1a), with *Cfs2*, a modulator of epithelial cell homeostasis, as well as classical M1 macrophage activation (28, 29), as likely inhibiting canonical pathways in the colons of *C. rodentium*-infected F₂ *Gif^{tm1a/tm1a}* mice (see Dataset S1a). The top five functional gene categories in hepatic mRNA of *C. rodentium*-infected F₂ *Gif^{tm1a/tm1a}* mice were predicted to be related to cellular function and maintenance, movement, development, growth and proliferation, and signaling, with our analysis showing many of these associated genes relatively downregulated (see Dataset S1e). A key transcriptional regulator was predicted to be *Acox1* (see Dataset S1a).

Finally, IPA of the hepatic mRNA data of differentially expressed genes found in *S. Typhimurium* infected F₂ *Gif^{tm1a/tm1a}* mice was performed (see Dataset S1a and f in the supplemental material). Consistent with the other IPA analyses (see Dataset S1a), *Acox1* was predicted to be a key regulatory element. Functional and canonical pathway analysis identified differentially expressed genes as associated with lipid, drug, and carbohydrate metabolism; small-molecule biochemistry; and cellular development. IPA indicated that functional pathways associated with fatty acid metabolism were overactivated ($P = 4.39e^{-06}$; see Dataset S1e).

Blood metabolic profiling identifies F₂ *Gif^{tm1a/tm1a}* mice as having abnormal glycolytic pathways and cellular energy homeostasis pathways. To identify metabolites that might be influenced downstream of the changes in transcriptional patterns observed in the tissues of F₂ *Gif^{tm1a/tm1a}* mice, metabotyping was performed by nuclear magnetic resonance (NMR) spectroscopy of blood serum taken from F₂ *Gif^{tm1a/tm1a}* and wild-type mice before and after an *S. Typhimurium* challenge. By performing principal component analysis (PCA), a multivariate data analysis method, we could distinguish the blood serum metabolic profiles

TABLE 1 Summary of the relative metabolic differences in the blood serum of naive and *S. Typhimurium*-infected F₂ *Gif*^{tm1a/tm1a} and wild-type mice^{a,c}

Metabolite(s)	Chemical shift(s) (ppm)	Fold change(s) ^b	
		Naive	Infected
Fatty acids	Several	↓ -1.2	—, ↑ 1.4 ^c
Putrescine-cadaverine	1.75, 3.04; 1.48, 3.80	—	↑
Glucose	3.24, 3.46, 3.52, 3.73; 3.83, 3.88, 5.22	↓ -1.2	↓ -1.3
Fucose	1.22, 1.25, 3.44, 3.60, 3.80, 5.25	—	↓ -1.5
Acetate	1.93	↑	—
Alanine	1.49, 1.51, 3.81	↑	—
Taurine-betaine	3.27, 3.44; 3.25, 3.90	↑	↓ -1.3, -2 ^c
Citrate-aspartate	2.55, 2.67; 2.64, 2.70	↑ 1.2	—
Formate	8.47	↑	—
Glutamate-glutamine	(2.04, 2.12), (2.34, 2.39), 3.74; (2.00, 24.00, 2.48), 3.78	↓	—
Isoleucine	0.98, 1.01, 3.66	↓	—
Leucine	0.96, 1.72, 3.75	↓	↓ -1.6
Methylmalonate	1.22, 3.18	↑ 1.3	↑ 1.2
Phenylacetylglycine	3.68, 3.76, 7.40	↑	↑
Valine	1.01, 1.06, 2.29, 3.61	—	↑
Adipate	1.56, 2.17	—	—, ↑ 1.6 ^c
3-Hydroxybutyrate	1.21, (2.32, 2.42), 4.16	—	↓
Butyrate	0.89, 1.56, 2.15	—	↓
Lactate	1.34, 4.13	↑ 1.2	—
Pyruvate-succinate	2.39, 2.41	↑	—
Choline-phosphocholine-glycerophosphocholine	3.20, 3.21, 3.22	—	↑
Malate	(2.36, 2.42), (2.66, 2.70), 4.30	—	↑

^a Fold change, >1.2; *P* < 0.05.

^b Shown are fold (>1.2) and significant (*P* < 0.05) changes in metabolite levels in F₂ *Gif*^{tm1a/tm1a} and wild-type mice.

^c Shown are fold (>1.2) and significant (*P* < 0.05) changes in metabolite levels in naive versus *S. Typhimurium*-infected F₂ *Gif*^{tm1a/tm1a} mice. Symbols: —, no significant fold change (>1.2); ↑ or ↓, relative increase or decrease in metabolites from PCA loading plots. These levels were estimated from relative intensities (median) of ¹H NMR spectra following spectral normalization.

of naive (Fig. 5a), as well as *S. Typhimurium* infected (Fig. 5b) F₂ *Gif*^{tm1a/tm1a} and wild-type mice.

As expected, uninfected wild-type mice demonstrated blood metabolic patterns of normal cellular homeostasis, harboring higher levels of fatty acids and glucose (Table 1). In contrast, naive F₂ *Gif*^{tm1a/tm1a} mice harbored a metabolic profile with similarities to the Warburg effect (30). This profile included higher levels of lactate and lower quantities of glucose, indicating that lactic acid fermentation was occurring to generate energy for cellular homeostasis. We also identified biomarkers of alternative cellular energy sourcing such a decrease amount of fatty acids and an increased quantity of citrate-aspartate, metabolites commonly associated with increased glycolysis and acetyl-CoA production (Table 1; see Fig. S5, in the supplemental material). Furthermore, we observed a high level of methylmalonate, a known plasma marker of Cbl deficiency, in the blood of naive F₂ *Gif*^{tm1a/tm1a} mice, suggesting that Cbl deficiency could be disrupting the trichloroacetic acid (TCA) cycle (14, 15).

Next, we metabotyped blood serum from wild-type and F₂ *Gif*^{tm1a/tm1a} mice at day 9 after an *S. Typhimurium* challenge (Fig. 5b). *S. Typhimurium* is known to cover its metabolic needs during infection by upregulating host cell glycolysis and associated fatty acid beta-oxidation pathways (22, 31, 32), with the blood of infected wild-type mice harboring relatively higher levels

of metabolites indicative of beta oxidation activity such as 3-hydroxybutyrate and butyrate and adipate (Table 1). In contrast, challenged F₂ *Gif*^{tm1a/tm1a} mice exhibited biomarkers associated with severe changes in cellular energy homeostasis and glycolytic processes, as well as metabolic starvation (30, 33). We identified lower levels of blood sugars (glucose and fucose), with taurine (Table 1), and leucine, metabolites thought to regulate mairine skeletal function as well as glucose and lipid homeostasis (12, 34) reduced in the blood of infected F₂ *Gif*^{tm1a/tm1a} mice. We also observed biomarkers of increased acetyl-CoA and fatty acid synthesis (fatty acids, valine, and phenylacetylglycine), and increased oxidative stress (adipate, taurine-betaine, chlorine, and malate) (30). Furthermore, and comparative to their uninfected F₂ *Gif*^{tm1a/tm1a} counterparts, the plasma Cbl marker methylmalonate was observed at high levels in the blood metabolite profile of infected F₂ *Gif*^{tm1a/tm1a} mice (Table 1).

Cbl supplementation reverses the *S. Typhimurium* susceptibility of F₂ *Gif*^{tm1a/tm1a} mice. To evaluate if F₂ *Gif*^{tm1a/tm1a} Cbl deficiency was directly impacting their hypersusceptibility to *C. rodentium* and *S. Typhimurium* infection, we supplemented F₂ *Gif*^{tm1a/tm1a} mice with Cbl in a series of subcutaneous injections prior to a challenge and compared their susceptibility to an *S. Typhimurium* M525 challenge with that of untreated F₂ *Gif*^{tm1a/tm1a} mice. As expected, untreated F₂ *Gif*^{tm1a/tm1a} mice showed signs of

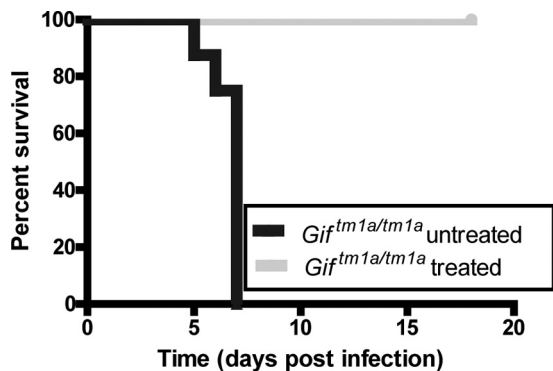


FIG 6 Cbl supplementation of F₂ *Gif*^{tm1a/tm1a} mice alters their susceptibility to an *S. Typhimurium* challenge. Shown is a Kaplan-Meier curve of percent survival of F₂ *Gif*^{tm1a/tm1a} mice left untreated or treated with cyanocobalamin and then infected with *S. Typhimurium* ($n = 8$).

salmonellosis by day 4 p.i. and had to be sacrificed by day 7 p.i. (Fig. 6). In contrast, equivalent Cbl-treated F₂ *Gif*^{tm1a/tm1a} mice exhibited limited signs of salmonellosis, survived the challenge, and were indistinguishable from their wild-type counterparts. Thus, Cbl deficiency in these F₂ *Gif*^{tm1a/tm1a} mice is likely directly influencing their susceptibility to *S. Typhimurium* infection.

DISCUSSION

By exploiting a novel *Gif* mutant mouse line, we have demonstrated a critical role for Cbl in controlling susceptibility to infection by two different bacterial pathogens, *C. rodentium* and *S. Typhimurium*. We link this severe phenotype to likely disruptions in glycolysis, fatty acid synthesis, and energy homeostasis processes in Cbl-defective mice (12, 14, 30, 31, 33), with infection susceptibility further being influenced by the genotype of mothers, a phenomenon linked to their ability to transfer Cbl to their offspring (35).

The results obtained with *Gif* deficient mice mimic aspects of the clinical phenotypes associated with Cbl deficiency in humans and other mammals. For example, children born to Cbl depleted mothers exhibit stunted growth (10), similar to that observed in F₂ *Gif*^{tm1a/tm1a} mice and infant rats and mice when Cbl was removed from their diet (16, 35, 36). Further, we demonstrate how Cbl deficiency can likely disrupt mammalian cellular homeostasis processes. F₂ *Gif*^{tm1a/tm1a} mice exhibited blood and histopathological signatures associated with DNA abnormalities such as megaloblastic anemia, abnormal mitotic figures, and cellular oxidative damage, phenotypes commonly associated with Cbl deficiency in humans and infant mice (8, 9, 11, 13). By metabolomic and transcriptional profiling, we also found evidence that succinyl-CoA, a Cbl by-product and an essential TCA cycle regulator, was inhibited in F₂ *Gif*^{tm1a/tm1a} mice, likely leading to increased glycolysis and fatty acid synthesis and other metabolic activities commonly associated with the Warburg effect (12–15, 30).

We were unable to detect a clear immunological signature associated with Cbl deficiency in F₂ *Gif*^{tm1a/tm1a} mice, even though others have reported that Cbl deficiency affects cytokine and T cell ratios in a uninfected host (37, 38). Clearly, we did not exhaustively screen for immune deficiencies, and further studies in this area are still warranted. However, the macrophage killing activity that is critical for controlling salmonellosis *in vivo* was not obviously impaired, and immune cell populations and cytokine levels

critical for *Salmonella* control appeared to be broadly similar (19). Interestingly however, and perhaps consistent with the Warburg effect (6), we did identify signatures for alternatively activated M2 macrophages, such as increased expression of arginase 1 by F₂ *Gif*^{tm1a/tm1a} mouse macrophages. We therefore concluded, like the authors of a previously published study (22), that this metabolic activation state has little impact on the control of *Salmonella* replication because these cells were still able to kill salmonellae *in vitro*.

After *C. rodentium* infection, F₂ *Gif*^{tm1a/tm1a} mice exhibited polymicrobial sepsis, with an overgrowth of *C. rodentium*. Histopathological examination revealed greater recruitment of inflammatory cells to the colon and liver than similarly infected wild-type mice, with transcriptional profiling suggesting that cellular homeostasis processes are likely disrupted in F₂ *Gif*^{tm1a/tm1a} mice after *C. rodentium* infection. F₂ *Gif*^{tm1a/tm1a} mice infected with *S. Typhimurium* exhibited greater signs of lethargy and morbidity, with severe histopathological damage. As *S. Typhimurium* utilizes the same fatty acid beta-oxidation and glycolysis pathways that are already dysregulated in F₂ *Gif*^{tm1a/tm1a} mice (22, 31, 32), we hypothesize that F₂ *Gif*^{tm1a/tm1a} mice are succumbing to *S. Typhimurium* infection from metabolic starvation, with their metabolomic and transcriptional profile strongly resembling this scenario (33).

This study has further highlighted some of the complex clinical and metabolomic abnormalities associated with Cbl deficiency, demonstrating the importance of Cbl in the mammalian diet. By performing studies on *Gif*^{tm1a/tm1a} or other mice with genetic defects associated with nutrient absorption, we can not only gain a better biological understanding of the interplay between nutritional regulation and the immune system but also further understand the pathogenesis associated with specific nutritional dysregulation.

MATERIALS AND METHODS

Animals. The *Gif*^{tm1a(KOMP)Wtsi} mouse line was generated on a C57BL/6N genetic background as part of the International Mouse Phenotyping Consortium (<http://www.mousephenotyping.org>). See Text S1 in the supplemental material for the gene targeting methods used to produce this mouse line. Animals were housed under specific-pathogen-free conditions in HEPA-filtered cages with sterile bedding and given a sterilized standard diet and water *ad libitum*. All experiments were performed in accordance with United Kingdom Animal (Scientific Procedures) Act 1986.

Hematology and blood chemistry analysis. Blood was collected under terminal anesthesia into either EDTA-coated tubes or heparinized tubes for plasma or serum preparation. Clinical chemistry analysis of plasma was performed with the Olympus AU400 analyzer (Beckman Coulter Ltd., High Wycombe, United Kingdom). Concentrations of Cbl in plasma were measured with the ADVIA Centaur immunoassay analyzer (Siemens).

Cbl treatment. Mice were treated subcutaneously with cyanocobalamin (Sigma Aldrich) at 1 mg/ml every 2 weeks for 6 weeks. Mice were left for 1 month before an *S. Typhimurium* infection challenge.

Cytokine analysis. Cytokine analysis was performed with the FlexMap 3D (Luminex) machine with a Milliplex Map Mouse Th17 Magnetic Bead Panel 96-well assay kit (Millipore). For method details, as well as a list of the cytokines analyzed, see Text S1 in the supplemental material.

Flow cytometry analysis. Analysis of peripheral blood leukocytes was performed with heparinized blood collected from 16-week-old mice. Peripheral blood leukocytes, mesenteric lymph nodes, and spleens were prepared and stained for flow cytometry analysis as described in Text S1 in the

supplemental material. All samples were analyzed on an LSR II or LSR Fortessa apparatus (BD Biosciences). Data were analyzed with FlowJo v9 software (TreeStar).

Histological analysis. For histological examination, 5- μ m sections of paraffin-embedded tissues were stained with hematoxylin and eosin (Sigma-Aldrich). Sections were examined and scored by a pathologist under blinded conditions. For immunohistochemistry analysis, sections were cut and fixed as described in Text S1 in the supplemental material. Sections were visualized by confocal microscopy (Leica).

NMR analysis. Blood serum was collected from age- and sex-matched mice (five per group), snap-frozen immediately, and stored at -80°C until analysis. Samples were analyzed with a Bruker ADVANCE III NMR spectrometer to identify metabolic differences between F₂ *Gif^{tm1a/tm1a}* and wild-type mice. For further details, see Text S1 in the supplemental material.

Microarray analysis. mRNA for microarray analysis was prepared as described in Text S1 in the supplemental material. Analysis was performed with the Illumina MouseWG-6 v2.0 Expression BeadChip kit. The data were analyzed with BeadStudio Software (Illumina) to identify genes differently regulated in F₂ *Gif^{tm1a/tm1a}* and wild-type mice. Further pathway analysis was performed by IPA (Qiagen, Redwood City, CA) of all of the genes differently expressed in F₂ *Gif^{tm1a/tm1a}* and wild-type mice ($P < 0.05$; log-fold change, 0.8). For further details of the IPA analysis performed, see Text S1 in the supplemental material.

RNA isolation and RT-qPCR of peritoneal macrophages. Resident peritoneal macrophages were isolated from naive mice by peritoneal lavage. RNA was isolated with the RNeasy minikit (Qiagen) and reverse transcribed with the QuantiTect reverse transcription (RT) kit (Qiagen). RT-quantitative PCR (RT-qPCR) experiments were performed as described in Text S1 in the supplemental material.

Mouse infection challenges. Background matched wild-type and *gif^{tm1a(KOMP)Wtsi}* mice 6 to 10 weeks of age were maintained in accordance with United Kingdom Home Office regulations under project license PPL80/2099 and 80/2596 (2596 replaced 2099 upon expiry). The Wellcome Trust Sanger Institute Ethical Review Committee has also reviewed this license. For *C. rodentium* challenges, mice were infected orally with 0.2 ml of *C. rodentium* ICC180. For *S. Typhimurium* challenges, mice were infected intravenously with a sublethal dose of *S. Typhimurium* M525. All mice were monitored daily for defined humane endpoints in accordance with United Kingdom Home Office license guidelines.

Measurement of pathogen burdens in organs. Organs were aseptically removed and homogenized mechanically. Viable counts were determined by serially diluting the organ homogenates onto LB agar plates for CFU counting.

Peritoneal macrophage gentamicin protection assay. Peritoneal macrophages were infected with *S. Typhimurium* M525 at a multiplicity of infection (MOI) of 20 for 1 h and then treated with gentamicin for another hour. Cells were then washed and incubated in antibiotic-free Opti-MEM (Thermo Fisher) for a further 5 h. For quantitative analysis, cells were lysed in 1% Triton X-100, serially diluted, and plated onto LB plates for CFU counting.

Statistical analysis. Where not already stated in Text S1 in the supplemental material, the Student *t* test was performed for experiments comparing two groups. For data with more than two groups, statistical analysis was performed by a nonparametric one-way analysis of variance (ANOVA) with Dunn's multiple-comparison *post hoc* test. For comparisons of groups with two or more factors, analysis was performed by two-way ANOVA with the Bonferroni multiple-comparison *posttest*. $P < 0.05$ was taken as significant in all cases. All tests were performed with GraphPad Prism 5 (GraphPad Software, Inc., La Jolla, CA).

Microarray data accession numbers. The microarray data associated with this paper are stored in the ArrayExpress public database (<http://www.ebi.ac.uk/arrayexpress>) under accession numbers E-MTAB-1879 and E-MTAB-1880.

SUPPLEMENTAL MATERIAL

Supplemental material for this article may be found at <http://mbio.asm.org/lookup/suppl/doi:10.1128/mBio.00830-16/-/DCSupplemental>.

Text S1, DOCX file, 0.2 MB.
Dataset S1, XLS file, 0.4 MB.
Figure S1, DOCX file, 0.7 MB.
Figure S2, DOCX file, 0.1 MB.
Figure S3, DOCX file, 2.4 MB.
Figure S4, DOCX file, 0.2 MB.
Figure S5, DOCX file, 0.3 MB.

ACKNOWLEDGMENTS

This work was supported by the Wellcome Trust via grant 098051.

We gratefully thank the Research Support Facility for animal maintenance and welfare. We also thank J. Choudhary for her helpful discussions.

L.M. and S.C. performed most of the experiments and analyzed the data. L.K., A.C., and C.B. assisted with mouse experiments. A.O.S., E.L.C., and Z.M. performed hematology, clinical chemistry, and blood flow analyses. G.S.V. and C.G. performed the blood serum Cbl and hematological analyses. R.M.S. performed the metabolomic metabotyping. S.M., M.A.D.-C., C.H., and J.F. performed the *in vitro* macrophage assays, staining of tissue, and cytokine analysis. M.A.D.-C. examined the histology. G.D. and B.W.W. oversaw the project. L.M., S.C., and G.D. wrote the manuscript.

FUNDING INFORMATION

This work, including the efforts of Lynda Mottram, Leanne Kane, Subhankar Mukhopadhyay, Amy Colin, Cordelia Brandt, Maria A. Duque-Correa, Jessica Forbester, Tu Anh Pham Nguyen, Christine Hale, Gordon Dougan, and Simon Clare, was funded by Wellcome Trust (098051).

REFERENCES

- Okoro CK, Kingsley RA, Quail MA, Kankwatira AM, Feasey NA, Parkhill J, Dougan G, Gordon MA. 2012. High-resolution single nucleotide polymorphism analysis distinguishes recrudescence and reinfection in recurrent invasive nontyphoidal *Salmonella typhimurium* disease. *Clin Infect Dis* 54:955–963. <http://dx.doi.org/10.1093/cid/cir1032>.
- Mondal D, Minak J, Alam M, Liu Y, Dai J, Korpe P, Liu L, Haque R, Petri WA, Jr. 2012. Contribution of enteric infection, altered intestinal barrier function, and maternal malnutrition to infant malnutrition in Bangladesh. *Clin Infect Dis* 54:185–192. <http://dx.doi.org/10.1093/cid/cir807>.
- Cunningham-Rundles S, McNeeley DF, Moon A. 2005. Mechanisms of nutrient modulation of the immune response. *J Allergy Clin Immunol* 115:1119–1128; quiz 1129. <http://dx.doi.org/10.1016/j.jaci.2005.04.036>.
- Maggini S, Wintergerst ES, Beveridge S, Hornig DH. 2007. Selected vitamins and trace elements support immune function by strengthening epithelial barriers and cellular and humoral immune responses. *Br J Nutr* 98(Suppl 1):S29–S35. <http://dx.doi.org/10.1017/S0007114507832971>.
- Rodríguez L, Cervantes E, Ortiz R. 2011. Malnutrition and gastrointestinal and respiratory infections in children: a public health problem. *Int J Environ Res Public Health* 8:1174–1205. <http://dx.doi.org/10.3390/ijerph8041174>.
- Kelly B, O'Neill LA. 2015. Metabolic reprogramming in macrophages and dendritic cells in innate immunity. *Cell Res* 25:771–784. <http://dx.doi.org/10.1038/cr.2015.68>.
- Martens JH, Barg H, Warren MJ, Jahn D. 2002. Microbial production of vitamin B₁₂. *Appl Microbiol Biotechnol* 58:275–285. <http://dx.doi.org/10.1007/s00253-001-0902-7>.
- Quadros EV. 2010. Advances in the understanding of cobalamin assimilation and metabolism. *Br J Haematol* 148:195–204. <http://dx.doi.org/10.1111/j.1365-2141.2009.07937.x>.
- O'Leary F, Samman S. 2010. Vitamin B₁₂ in health and disease. *Nutrients* 2:299–316. <http://dx.doi.org/10.3390/nu2030299>.
- Muthayya S, Kurpad AV, Duggan CP, Bosch RJ, Dwarkanath P, Mhaskar A, Mhaskar R, Thomas A, Vaz M, Bhat S, Fawzi WW. 2006. Low maternal vitamin B₁₂ status is associated with intrauterine growth

- retardation in urban south Indians. *Eur J Clin Nutr* 60:791–801. <http://dx.doi.org/10.1038/sj.ejcn.1602383>.
11. Aslinia F, Mazza JJ, Yale SH. 2006. Megaloblastic anemia and other causes of macrocytosis. *Clin Med Res* 4:236–241. <http://dx.doi.org/10.3121/cmr.4.3.236>.
 12. Green CR, Wallace M, Divakaruni AS, Phillips SA, Murphy AN, Ciaraldi TP, Metallo CM. 2016. Branched-chain amino acid catabolism fuels adipocyte differentiation and lipogenesis. *Nat Chem Biol* 12:15–21. <http://dx.doi.org/10.1038/nchembio.1961>.
 13. Ahmad S, Kumar KA, Basak T, Bhardwaj G, Yadav DK, Lalitha A, Chandak GR, Raghunath M, Sengupta S. 2013. PPAR signaling pathway is a key modulator of liver proteome in pups born to vitamin B(12) deficient rats. *J Proteomics* 91:297–308. <http://dx.doi.org/10.1016/j.jpropt.2013.07.027>.
 14. Frenkel EP, Kitchens RL, Johnston JM. 1973. The effect of vitamin B₁₂ deprivation on the enzymes of fatty acid synthesis. *J Biol Chem* 248:7450–7456.
 15. Tanpaiboon P. 2005. Methylmalonic acidemia (MMA). *Mol Genet Metab* 85:2–6.
 16. Roman-García P, Quiros-Gonzalez I, Mottram L, Lieben L, Sharan K, Wangwiwatsin A, Tubio J, Lewis K, Wilkinson D, Santhanam B, Sarper N, Clare S, Vassiliou GS, Velagapudi VR, Dougan G, Yadav VK. 2014. Vitamin B₁₂-dependent taurine synthesis regulates growth and bone mass. *J Clin Invest* 124:2988–3002. <http://dx.doi.org/10.1172/JCI72606>.
 17. White JK, Gerdin AK, Karp NA, Ryder E, Buljan M, Bussell JN, Salisbury J, Clare S, Ingham NJ, Podrini C, Houghton R, Estabel J, Bottomley JR, Melvin DG, Sunter D, Adams NC, Sanger Institute Mouse Genetics Project, Tannahill D, Logan DW, Macarthur DG, Flint J, Mahajan VB, Tsang SH, Smyth I, Watt FM, Skarnes WC, Dougan G, Adams DJ, Ramirez-Solis R, Bradley A, Steel KP. 2013. Genome-wide generation and systematic phenotyping of knockout mice reveals new roles for many genes. *Cell* 154:452–464. <http://dx.doi.org/10.1016/j.cell.2013.06.022>.
 18. Schatten H, Wiedemeier AM, Taylor M, Lubahn DB, Greenberg NM, Besch-Williford C, Rosenfeld CS, Day JK, Ripple M. 2000. Centrosome-centriole abnormalities are markers for abnormal cell divisions and cancer in the transgenic adenocarcinoma mouse prostate (TRAMP) model. *Biol Cell* 92:331–340. [http://dx.doi.org/10.1016/S0248-4900\(00\)01079-0](http://dx.doi.org/10.1016/S0248-4900(00)01079-0).
 19. Dougan G, John V, Palmer S, Mastroeni P. 2011. Immunity to salmonellosis. *Immunol Rev* 240:196–210. <http://dx.doi.org/10.1111/j.1600-065X.2010.00999.x>.
 20. Monack DM, Raupach B, Hromockyj AE, Falkow S. 1996. Salmonella typhimurium invasion induces apoptosis in infected macrophages. *Proc Natl Acad Sci U S A* 93:9833–9838. <http://dx.doi.org/10.1073/pnas.93.18.9833>.
 21. Sheppard M, Webb C, Heath F, Mallows V, Emilianus R, Maskell D, Mastroeni P. 2003. Dynamics of bacterial growth and distribution within the liver during salmonella infection. *Cell Microbiol* 5:593–600. <http://dx.doi.org/10.1046/j.1462-5822.2003.00296.x>.
 22. Eisele NA, Ruby T, Jacobson A, Manzanillo PS, Cox JS, Lam L, Mukundan L, Chawla A, Monack DM. 2013. Salmonella require the fatty acid regulator PPARdelta for the establishment of a metabolic environment essential for long-term persistence. *Cell Host Microbe* 14:171–182. <http://dx.doi.org/10.1016/j.chom.2013.07.010>.
 23. Otto DM, Henderson CJ, Carrie D, Davey M, Gundersen TE, Blomhoff R, Adams RH, Tickle C, Wolf CR. 2003. Identification of novel roles of the cytochrome P450 system in early embryogenesis: effects on vasculogenesis and retinoic acid homeostasis. *Mol Cell Biol* 23:6103–6116. <http://dx.doi.org/10.1128/MCB.23.17.6103-6116.2003>.
 24. Li MD, Li CM, Wang Z. 2012. The role of circadian clocks in metabolic disease. *Yale J Biol Med* 85:387–401.
 25. Fournier B, Saudubray JM, Benichou B, Lyonnet S, Munnich A, Clevers H, Poll-The BT. 1994. Large deletion of the peroxisomal acyl-CoA oxidase gene in pseudoneonatal adrenoleukodystrophy. *J Clin Invest* 94:526–531. <http://dx.doi.org/10.1172/JCI117365>.
 26. Li Y, Tharappel JC, Cooper S, Glenn M, Glauert HP, Spear BT. 2000. Expression of the hydrogen peroxide-generating enzyme fatty acyl CoA oxidase activates NF-kappaB. *DNA Cell Biol* 19:113–120. <http://dx.doi.org/10.1089/104454900314627>.
 27. Kabashima K, Saji T, Murata T, Nagamachi M, Matsuoka T, Segi E, Tsuboi K, Sugimoto Y, Kobayashi T, Miyachi Y, Ichikawa A, Narumiya S. 2002. The prostaglandin receptor EP4 suppresses colitis, mucosal damage and CD4 cell activation in the gut. *J Clin Invest* 109:883–893. <http://dx.doi.org/10.1172/JCI14459>.
 28. Enzler T, Gillessen S, Manis JP, Ferguson D, Fleming J, Alt FW, Mihm M, Dranoff G. 2003. Deficiencies of GM-CSF and interferon gamma link inflammation and cancer. *J Exp Med* 197:1213–1219. <http://dx.doi.org/10.1084/jem.20021258>.
 29. Dongari-Bagtzoglou A, Kashleva H. 2003. Granulocyte-macrophage colony-stimulating factor responses of oral epithelial cells to *Candida albicans*. *Oral Microbiol Immunol* 18:165–170. <http://dx.doi.org/10.1034/j.1399-302X.2003.00061.x>.
 30. Vander Heiden MG, Cantley LC, Thompson CB. 2009. Understanding the Warburg effect: the metabolic requirements of cell proliferation. *Science* 324:1029–1033. <http://dx.doi.org/10.1126/science.1160809>.
 31. Arsenault RJ, Napper S, Kogut MH. 2013. *Salmonella enterica* Typhimurium infection causes metabolic changes in chicken muscle involving AMPK, fatty acid and insulin/mTOR signaling. *Vet Res* 44:35. <http://dx.doi.org/10.1186/1297-9716-44-35>.
 32. Antunes LC, Arena ET, Menendez A, Han J, Ferreira RB, Buckner MM, Lolić P, Madilao LL, Bohlmann J, Borchers CH, Finlay BB. 2011. Impact of salmonella infection on host hormone metabolism revealed by metabolomics. *Infect Immun* 79:1759–1769. <http://dx.doi.org/10.1128/IAI.01373-10>.
 33. Lempradl A, Pospisilik JA, Penninger JM. 2015. Exploring the emerging complexity in transcriptional regulation of energy homeostasis. *Nat Rev Genet* 16:665–681. <http://dx.doi.org/10.1038/nrg3941>.
 34. De Luca A, Pierno S, Camerino DC. 2015. Taurine: the appeal of a safe amino acid for skeletal muscle disorders. *J Transl Med* 13:243. <http://dx.doi.org/10.1186/s12967-015-0610-1>.
 35. Hellegers A, Okuda K, Nesbitt RE, Jr., Smith DW, Chow BF. 1957. Vitamin B₁₂ absorption in pregnancy and in the newborn. *Am J Clin Nutr* 5:327–331.
 36. Molina V, Medici M, Taranto MP, Font de Valdez G. 2008. Effects of maternal vitamin B₁₂ deficiency from end of gestation to weaning on the growth and haematological and immunological parameters in mouse dams and offspring. *Arch Anim Nutr* 62:162–168. <http://dx.doi.org/10.1080/17450390801892567>.
 37. Funada U, Wada M, Kawata T, Mori K, Tamai H, Isshiki T, Onoda J, Tanaka N, Tadokoro T, Maekawa A. 2001. Vitamin B-12-deficiency affects immunoglobulin production and cytokine levels in mice. *Int J Vitam Nutr Res* 71:60–65. <http://dx.doi.org/10.1024/0300-9831.71.1.60>.
 38. Tamura J, Kubota K, Murakami H, Sawamura M, Matsushima T, Tamura T, Saitoh T, Kurabayashi H, Naruse T. 1999. Immunomodulation by vitamin B₁₂: augmentation of CD8⁺ T lymphocytes and natural killer (NK) cell activity in vitamin B₁₂-deficient patients by methyl-B₁₂ treatment. *Clin Exp Immunol* 116:28–32. <http://dx.doi.org/10.1046/j.1365-2249.1999.00870.x>.